Mechanics of Materials 191 (2024) 104954

Contents lists available at ScienceDirect

Mechanics of Materials

journal homepage: www.elsevier.com/locate/mecmat

Research paper

An analytical model of reactive diffusion for transient electronics with thick encapsulation layer

Haohui Zhang [a], Kaiqing Zhang [a,b], John A. Rogers [c,d,e,f], Yonggang Huang [a,c,d,g,*]

[a] Department of Civil and Environmental Engineering, Northwestern University, Evanston, 60208, IL, USA
[b] State Key Laboratory of Structural Analysis, Optimization and CAE Software for Industrial Equipment, Department of Engineering Mechanics, Dalian University of Technology, Dalian, 116024, Liaoning, China
[c] Departments of Materials Science and Engineering, Northwestern University, Evanston, 60208, IL, USA
[d] Querrey Simpson Institute for Bioelectronics, Northwestern University, Evanston, 60208, IL, USA
[e] Departments of Biomedical Engineering, Northwestern University, Evanston, 60208, IL, USA
[f] Departments of Neurological Surgery, Northwestern University, Chicago, 60611, IL, USA
[g] Departments of Mechanical Engineering, Northwestern University, Evanston, 60208, IL, USA

ARTICLE INFO

Keywords:
Reactive diffusion model
Analytical solution
Scaling law
Transient electronics
Encapsulation layer

ABSTRACT

Transient electronic systems are engineered to physically disappear after a predetermined period. Such systems hold significant promise for environmental sustainability and medical applications. The transient behavior relies on the interplay between water diffusion and the hydrolysis reaction of the device components, with the thickness of the encapsulation layer serving as a crucial parameter for controlling the lifetime of the device. The established analytical model for reactive diffusion, however, is limited to relatively thin encapsulation layers. We extend the analytical model to thick encapsulation layers in order to predict transient electronics' lifetimes for both thin and thick encapsulation layers, broadening its applicability. Furthermore, we obtain a scaling law between the dissolution time and the dissolved thickness of transient electronics for the limit of a thick encapsulation layer with no reaction. This scaling law offers a robust way for calculating the dissolution time across different device configurations.

1. Introduction

Traditional electronic systems are engineered for longevity, emphasizing stable performance over extended periods with minimal change. On the opposite, the transient electronic system, as proposed by Hwang et al. (2012), embraces a fundamentally different philosophy. These systems are designed for a controllable, finite duration of functionality with an inherent capacity to degrade and dissolve in aqueous environments at predetermined durations and rates. This unique characteristic offers advantages in two scenarios. Firstly, it enables these devices to physically disappear in the external environment, mitigating environmental impact and eliminating the costs and health risks associated with discarded electronics (Burns et al., 2016; Heacock et al., 2016; Fu et al., 2016; Huang et al., 2014; Jung et al., 2015; Irimia-Vladu et al., 2010). Secondly, when used in biomedical contexts, such devices can be bioresorbed by the body, obviating the need for secondary surgical procedures to remove implants. Consequently, transient electronics have found widespread application in the medical field, serving as implantable diagnostic tools, interventional components, and therapeutic delivery vehicles (Jia et al., 2016; Yu et al., 2016; Kang et al., 2016; Lee et al., 2015; Tao et al., 2014; Won et al., 2018).

In the realm of transient electronics, a variety of degradable materials have been explored to match the performance of conventional electronic devices. For semiconductors, silicon nanomembrane (SiNM) is a preferred choice. Its hydrolysis in phosphate-buffered saline (PBS) (pH = 7.4, physiological levels) forms silicic acid ($Si(OH)_4$) through the reaction $Si + 4H_2O \longleftrightarrow Si(OH)_4 + 2H_2$ (Krauskopf, 1956; Iler, 1973; Rimstidt and Barnes, 1980). Although silicon's hydrolysis rate is relatively slow, its thinness compensates, making the dissolution time acceptable. Several metals are used as conductors. For conductive elements, magnesium (Mg) stands out due to its ease of processing, biocompatibility, and rapid hydrolysis, producing $Mg(OH)_2$ in physiological conditions (Hwang et al., 2012; Yin et al., 2014; Zeng et al., 2008; Witte, 2010). Other metals like zinc (Zn), iron (Fe), tungsten (W), and molybdenum (Mo) offer similar benefits (Yin et al., 2014; Mueller et al., 2012; Hermawan et al., 2010; Nie et al., 2010; Bowen et al., 2013; Patrick et al., 2011; Badawy and Al-Kharafi, 1998), with most being essential for biological functions. In the context of dielectrics,

* Corresponding author at: Department of Civil and Environmental Engineering, Northwestern University, Evanston, 60208, IL, USA.
E-mail address: y-huang@northwestern.edu (Y. Huang).

https://doi.org/10.1016/j.mechmat.2024.104954
Received 29 January 2024; Received in revised form 17 February 2024; Accepted 19 February 2024
Available online 21 February 2024

magnesium oxide (MgO) and silicon dioxide (SiO_2) are utilized. They react with water to form dissolvable $Mg(OH)_2$ and $Si(OH)_4$, respectively (Amaral et al., 2010; Wetteland et al., 2018; Kang et al., 2014; Lee et al., 2017). Furthermore, biodegradable polymers such as polylactic acid (PLA), poly(lactic-co-glycolic acid) (PLGA), polyanhydride (PA), natural wax, and silk fibroin are employed as substrates and packaging materials (Place et al., 2009; Choi et al., 2020). Their dissolution rates are crucial, not only for their own disintegration but also for serving as a barrier against water, thereby protecting other device components. This setup allows precise control over the dissolution rate of functional parts by selecting appropriate polymers and designing suitable geometries. The polymers' interaction with water varies significantly; some are hydrophilic with high water permeability (Place et al., 2009), while others are hydrophobic, effectively repelling water for extended periods (Won et al., 2018; Choi et al., 2020). Consequently, the stable operational duration of these transient electronic devices can be meticulously controlled, ranging from hours to months.

The lifetime of transient electronic devices is predominantly governed by the interplay of diffusion and hydrolysis reactions within the system. Initially, water molecules permeate the encapsulation layer, undergoing simultaneous reactions and diffusion. Subsequently, these molecules diffuse into the functional components, such as magnesium (Mg), and initiate reactions that gradually impair the device's functionality. To comprehend and accurately predict the lifetime of these devices, the reactive diffusion model was introduced by Li et al. (2013). This model, considering a MgO encapsulation layer and a Mg electrical circuit, calculated the diminishing thickness of the Mg layer over time. As the Mg layer thins, the device's resistance increases, leading to functional loss, which is defined as the device's lifetime. This model has been validated through successful correlation with experimental results (Hwang et al., 2012; Won et al., 2018; Choi et al., 2020). However, a limitation arises from the original model's focus on scenarios where the encapsulation layer is thin, comparable in thickness to the Mg layer. In practical applications, the encapsulation layer is often substantially thicker to ensure extended device lifetime. In such cases, the diffusion within the encapsulation layer becomes the critical time-controlling factor, overshadowing the relatively rapid reaction in the conductive Mg layer. This discrepancy highlights the need for an expanded model that accurately represents devices with thicker encapsulation layers, a gap that our current work aims to address.

In response to this identified need, our study offers an analytical solution to the reactive diffusion model that accommodates both thin and thick encapsulation layers in transient electronic devices. Then we derive a scaling law for the thick encapsulation layer, where the diffusion in the encapsulation layer is the control factor of the whole process. This scaling law emphasizes the diffusion in the encapsulation layer as the primary determinant of the device's dissolution process. It provides a simple tool for understanding and predicting the lifetime of transient electronics under diverse conditions.

2. Double-layer reactive diffusion model

The device comprises a bottom magnesium (Mg) layer and an encapsulation layer on top (Fig. 1). The top surface contacts the water bath. Given that the thicknesses of both layers are typically much smaller than their widths and lengths, a one-dimensional reactive diffusion model is an appropriate simplification for our analysis.

The mass conservation equations for both the Mg and the encapsulation layers are (Li et al., 2013)

$$D\frac{\partial^2 w}{\partial z^2} - kw - \frac{\partial w}{\partial t} = 0, \qquad 0 < z < h_0 \tag{1a}$$

$$D_{en}\frac{\partial^2 w}{\partial z^2} - k_{en}w - \frac{\partial w}{\partial t} = 0, \qquad h_0 < z < h_0 + h_{en} \tag{1b}$$

where w is the concentration of water which is the function of position z and time t; D, k, h_0, D_{en}, k_{en}, and h_{en} are the diffusivity, hydrolysis reaction constant, and initial thickness of the Mg and encapsulation layers, respectively.

We introduce the following nondimensional variables and parameters:

$$\widetilde{z} = z/h_0, \qquad \widetilde{t} = Dt/h_0^2, \qquad \widetilde{w} = w/w_0, \qquad \widetilde{k} = kh_0^2/D,$$
$$\widetilde{h}_{en} = h_{en}/h_0, \qquad \widetilde{D}_{en} = D_{en}/D, \qquad \widetilde{k}_{en} = k_{en}h_0^2/D \tag{2}$$

where w_0 is the water mass concentration in the water bath.

In the subsequent text, for simplicity, we will omit all $\widetilde{}$ notation. The nondimensional mass conservation equations Eq. (1) then become

$$\frac{\partial^2 w}{\partial z^2} - kw - \frac{\partial w}{\partial t} = 0, \qquad 0 < z < 1 \tag{3a}$$

$$D_{en}\frac{\partial^2 w}{\partial z^2} - k_{en}w - \frac{\partial w}{\partial t} = 0, \qquad 1 < z < 1 + h_{en} \tag{3b}$$

The device is immersed in water. Its top surface has the same water concentration w_0 as the water bath. Its bottom, in contact with the substrate, has zero flux. In addition, both the concentration of water and its flux are continuous across the interface between the Mg layer and the encapsulation layer. These are expressed as follows:

$$w|_{z=1+h_{en}} = 1 \tag{4a}$$

$$\frac{\partial w}{\partial z}|_{z=0} = 0 \tag{4b}$$

$$w|_{z=1^-} = w|_{z=1^+} \tag{4c}$$

$$\frac{\partial w}{\partial z}|_{z=1^-} = D_{en}\frac{\partial w}{\partial z}|_{z=1^+} \tag{4d}$$

At $t = 0$, both the Mg layer and the encapsulation layer are devoid of water:

$$w|_{t=0} = 0 \tag{5}$$

The solution can be expressed as the sum of a steady state solution w_s, which holds for $t \to \infty$, and a transient part w_h that depends on both z and t:

$$w(z,t) = w_s(z) + w_h(z,t) \tag{6}$$

The steady state solution w_s also satisfies Eqs. (3) and (4), and is given by

$$w_s = \begin{cases} P\cosh(\sqrt{k}z), & 0 < z < 1 \\ \cosh\left[\sqrt{\frac{k_{en}}{D_{en}}}(1 + h_{en} - z)\right] + Q\sinh\left[\sqrt{\frac{k_{en}}{D_{en}}}(1 + h_{en} - z)\right], & 1 < z < 1 + h_{en} \end{cases} \tag{7}$$

where

$$1/P = \cosh(\sqrt{k})\cosh\left(\sqrt{\frac{k_{en}}{D_{en}}}h_{en}\right) + \sqrt{\frac{k}{k_{en}D_{en}}}\sinh(\sqrt{k})\sinh\left(\sqrt{\frac{k_{en}}{D_{en}}}h_{en}\right) \tag{8a}$$

$$Q = -\frac{\sqrt{\frac{k}{k_{en}D_{en}}}\tanh(\sqrt{k}) + \tanh\left(\sqrt{\frac{k_{en}}{D_{en}}}h_{en}\right)}{1 + \sqrt{\frac{k}{k_{en}D_{en}}}\tanh(\sqrt{k})\tanh\left(\sqrt{\frac{k_{en}}{D_{en}}}h_{en}\right)} \tag{8b}$$

The transient solution w_h also satisfies Eqs. (3) and (4), except Eq. (4a) is revised to

$$w_h|_{z=1+h_{en}} = 0 \tag{9}$$

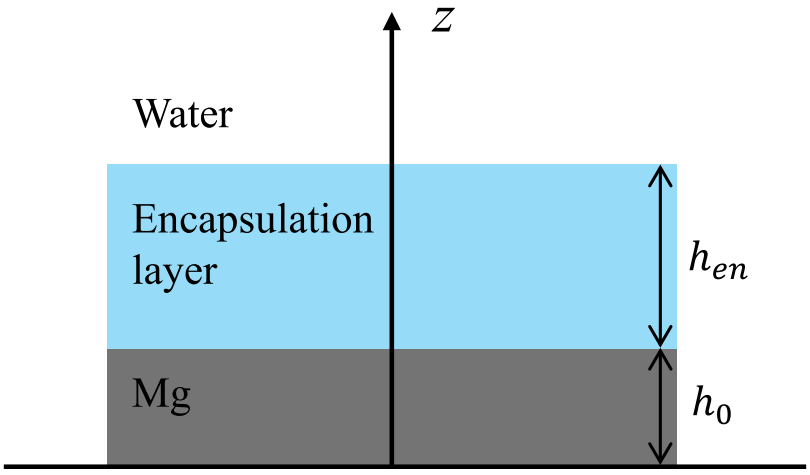

Fig. 1. Schematic of the device for reactive diffusion model.

w_h can be solved by the method of separation of variables:

$$w_h(z,t) = Z(z)T(t) \tag{10}$$

which gives

$$\frac{Z''}{Z} - k = \frac{T'}{T} = -\lambda, \qquad 0 < z < 1 \tag{11a}$$

$$D_{en}\frac{Z''}{Z} - k_{en} = \frac{T'}{T} = -\lambda, \qquad 1 < z < 1 + h_{en} \tag{11b}$$

where the constant λ is the eigenvalue to be determined. The solution of T to Eq. (11a) is

$$T = e^{-\lambda t} \tag{12}$$

For a thin encapsulation layer, the eigenvalues λ are always larger than both k and k_{en}, and this has been studied by Li et al. (2013) and is summarized below. For a relatively thick encapsulation layer, the eigenvalue λ could be between k or k_{en} (though never smaller than both k and k_{en}), as studied below.

2.1. $\lambda > max(k, k_{en})$

The solution of Z to Eq. (11a) is (Li et al., 2013)

$$Z = A\cos(\sqrt{\lambda - k}z), \qquad 0 < z < 1 \tag{13a}$$

$$Z = F\sin\left[\sqrt{\frac{\lambda - k_{en}}{D_{en}}}(1 + h_{en} - z)\right], \qquad 1 < z < 1 + h_{en} \tag{13b}$$

which already satisfies the boundary conditions Eqs. (9) and (4b). The constants A and F are to be determined from the continuity conditions Eqs. (4c) and (4d):

$$\begin{bmatrix} \cos(\sqrt{\lambda - k}) & -\sin\left(\sqrt{\frac{\lambda - k_{en}}{D_{en}}}h_{en}\right) \\ -\sqrt{\lambda - k}\sin(\sqrt{\lambda - k}) & \sqrt{(\lambda - k_{en})D_{en}}\cos\left(\sqrt{\frac{\lambda - k_{en}}{D_{en}}}h_{en}\right) \end{bmatrix} \begin{bmatrix} A \\ F \end{bmatrix} = \begin{bmatrix} 0 \\ 0 \end{bmatrix} \tag{14}$$

To ensure a non-trivial solution, the determinant of the coefficient matrix above must be zero, which leads to the eigenequation:

$$\sqrt{\frac{(\lambda - k_{en})D_{en}}{\lambda - k}}\cos(\sqrt{\lambda - k})\cos\left(\sqrt{\frac{\lambda - k_{en}}{D_{en}}}h_{en}\right) - \sin(\sqrt{\lambda - k})\sin\left(\sqrt{\frac{\lambda - k_{en}}{D_{en}}}h_{en}\right) = 0 \tag{15}$$

or equivalently

$$\tan(\sqrt{\lambda - k})\tan\left(\sqrt{\frac{\lambda - k_{en}}{D_{en}}}h_{en}\right) = \sqrt{\frac{(\lambda - k_{en})D_{en}}{\lambda - k}} \tag{16}$$

Its solution gives the eigenvalues, denoted as $\lambda_{n,1}$ (where $n = 1, 2, 3, \ldots$). For each eigenvalue $\lambda_{n,1}$, the associated eigenfunction is

$$f_{n,1}(z) = \begin{cases} \sin\left(\sqrt{\frac{\lambda_{n,1} - k_{en}}{D_{en}}}h_{en}\right)\cos(\sqrt{\lambda_{n,1} - k}z), & 0 < z < 1 \\ \cos(\sqrt{\lambda_{n,1} - k})\sin\left[\sqrt{\frac{\lambda_{n,1} - k_{en}}{D_{en}}}(1 + h_{en} - z)\right], & 1 < z < 1 + h_{en} \end{cases} \tag{17}$$

2.2. λ between k and k_{en}

Two mutually exclusive cases are considered below. Their eigenvalues are both called $\lambda_{n,2}$.

2.2.1. $k > k_{en}$

The process is the same as outlined in 2.1. We directly present the eigenequation:

$$\sqrt{\frac{(\lambda - k_{en})D_{en}}{k - \lambda}}\cosh(\sqrt{k - \lambda})\cos\left(\sqrt{\frac{\lambda - k_{en}}{D_{en}}}h_{en}\right) + \sinh(\sqrt{k - \lambda})\sin\left(\sqrt{\frac{\lambda - k_{en}}{D_{en}}}h_{en}\right) = 0 \tag{18}$$

or equivalently

$$\tanh(\sqrt{k - \lambda})\tan\left(\sqrt{\frac{\lambda - k_{en}}{D_{en}}}h_{en}\right) = -\sqrt{\frac{(\lambda - k_{en})D_{en}}{k - \lambda}} \tag{19}$$

Its solution (eigenvalue) between k and k_{en} is denoted by $\lambda_{n,2}$. The eigenfunction for this case is

$$f_{n,2}(z) = \begin{cases} \sin\left(\sqrt{\frac{\lambda_{n,2} - k_{en}}{D_{en}}}h_{en}\right)\cosh(\sqrt{k - \lambda_{n,2}}z), & 0 < z < 1 \\ \cosh(\sqrt{k - \lambda_{n,2}})\sin\left[\sqrt{\frac{\lambda_{n,2} - k_{en}}{D_{en}}}(1 + h_{en} - z)\right], & 1 < z < 1 + h_{en} \end{cases} \tag{20}$$

$$C_{n,1} = -\frac{2\sqrt{(\lambda_{n,1}-k_{en})D_{en}}\cos(\sqrt{\lambda_{n,1}-k})/\lambda_{n,1}}{\sin^2\left(\sqrt{\frac{\lambda_{n,1}-k_{en}}{D_{en}}}h_{en}\right)\left[1+\frac{\sin(2\sqrt{\lambda_{n,1}-k})}{2\sqrt{\lambda_{n,1}-k}}\right]+\cos^2(\sqrt{\lambda_{n,1}-k})\left[h_{en}-\frac{\sin\left(2\sqrt{\frac{\lambda_{n,1}-k_{en}}{D_{en}}}h_{en}\right)}{2\sqrt{\frac{\lambda_{n,1}-k_{en}}{D_{en}}}}\right]} \tag{27}$$

where $\lambda_{n,1}$ is solved by Eq. (15).

$$C_{n,2} = -\frac{2\sqrt{(\lambda_{n,2}-k_{en})D_{en}}\cosh(\sqrt{k-\lambda_{n,2}})/\lambda_{n,2}}{\sin^2\left(\sqrt{\frac{\lambda_{n,2}-k_{en}}{D_{en}}}h_{en}\right)\left[1+\frac{\sinh(2\sqrt{k-\lambda_{n,2}})}{2\sqrt{k-\lambda_{n,2}}}\right]+\cosh^2(\sqrt{k-\lambda_{n,2}})\left[h_{en}-\frac{\sin\left(2\sqrt{\frac{\lambda_{n,2}-k_{en}}{D_{en}}}h_{en}\right)}{2\sqrt{\frac{\lambda_{n,2}-k_{en}}{D_{en}}}}\right]}, \quad k > k_{en} \tag{28}$$

where $\lambda_{n,2}$ is solved by Eq. (18).

$$C_{n,2} = -\frac{2\sqrt{(k_{en}-\lambda_{n,2})D_{en}}\cos(\sqrt{\lambda_{n,2}-k})/\lambda_{n,2}}{\sinh^2\left(\sqrt{\frac{k_{en}-\lambda_{n,2}}{D_{en}}}h_{en}\right)\left[1+\frac{\sin(2\sqrt{\lambda_{n,2}-k})}{2\sqrt{\lambda_{n,2}-k}}\right]+\cos^2(\sqrt{\lambda_{n,2}-k})\left[-h_{en}+\frac{\sinh\left(2\sqrt{\frac{k_{en}-\lambda_{n,2}}{D_{en}}}h_{en}\right)}{2\sqrt{\frac{k_{en}-\lambda_{n,2}}{D_{en}}}}\right]}, \quad k < k_{en} \tag{29}$$

where $\lambda_{n,2}$ is solved by Eq. (21).

Box I.

2.2.2. $k < k_{en}$

The eigenequation is

$$\sqrt{\frac{(k_{en}-\lambda)D_{en}}{\lambda-k}}\cos(\sqrt{\lambda-k})\cosh\left(\sqrt{\frac{k_{en}-\lambda}{D_{en}}}h_{en}\right) - \sin(\sqrt{\lambda-k})\sinh\left(\sqrt{\frac{k_{en}-\lambda}{D_{en}}}h_{en}\right) = 0 \tag{21}$$

or equivalently

$$\tan(\sqrt{\lambda-k})\tanh\left(\sqrt{\frac{k_{en}-\lambda}{D_{en}}}h_{en}\right) = \sqrt{\frac{(k_{en}-\lambda)D_{en}}{\lambda-k}} \tag{22}$$

Its solution (eigenvalue) between k and k_{en} is denoted by $\lambda_{n,2}$. The eigenfunction for this case is

$$f_{n,2}(z) = \begin{cases} \sinh\left(\sqrt{\frac{k_{en}-\lambda_{n,2}}{D_{en}}}h_{en}\right)\cos(\sqrt{\lambda_{n,2}-k}z), & 0 < z < 1 \\ \cos(\sqrt{\lambda_{n,2}-k})\sinh\left[\sqrt{\frac{k_{en}-\lambda_{n,2}}{D_{en}}}(1+h_{en}-z)\right], & 1 < z < 1+h_{en} \end{cases} \tag{23}$$

2.3. General solution

The transient solution w_h is

$$w_h = \sum_{i=1,2;n=1,2,3,\ldots} C_{n,i}e^{-\lambda_{n,i}t}f_{n,i}(z) \tag{24}$$

where the coefficient $C_{n,i}$ is to be determined by the initial condition Eq. (5):

$$\sum_{i=1,2;n=1,2,3,\ldots} C_{n,i}f_{n,i}(z) + w_s = 0 \tag{25}$$

The orthogonality of eigenfunctions gives $C_{n,i}$ as

$$C_{n,i} = -\frac{\int_0^{1+h_{en}} f_{n,i}w_s\mathrm{d}z}{\int_0^{1+h_{en}} f_{n,i}^2\mathrm{d}z} \tag{26}$$

which yields (see Eqs. (27)–(29) in Box I).

2.4. Conditions for solutions exclusively with $\lambda > max(k, k_{en})$

The case where $\lambda > max(k, k_{en})$ always yields an infinite number of eigenvalues. However, eigenequations for other cases may not always have roots. To address these nuances, it is essential to discuss each case individually.

For $k_{en} < \lambda < k$, the condition for Eq. (18) to have no root is

$$h_{en} < \frac{\pi}{2}\sqrt{\frac{D_{en}}{k-k_{en}}} \tag{30}$$

For $k < \lambda < k_{en}$, there are two conditions for Eq. (21) to have no root:

$$0 < k_{en} - k < \pi^2/4 \tag{31a}$$

$$h_{en} < \frac{D_{en}}{\sqrt{k_{en}-k}\tan\sqrt{k_{en}-k}} \tag{31b}$$

It is clear that the study by Li et al. (2013) holds for a thin encapsulation layer (small h_{en}) such that Eq. (30) holds.

2.5. Thickness decrease of Mg layer

The equation governing the thickness change of the Mg layer is (Li et al., 2013)

$$\frac{\mathrm{d}h}{\mathrm{d}t} = \frac{Mw_0}{q\rho M_w}k\int_0^1 w\mathrm{d}z \tag{32}$$

where M and M_w are the molar masses of Mg and water, respectively. ρ is the mass density of the Mg. q is the number of water molecules required to hydrolyze one Mg molecule. Substitution of w in Eqs. (6), (7) and (24) into the above integration gives the thickness $h(t)$ of the Mg layer as

$$h(t) = 1 - \frac{Mw_0}{q\rho M_w}k\left[Pt\frac{\sinh(\sqrt{k})}{\sqrt{k}} + \sum_n \frac{C_{n,1}}{\lambda_{n,1}}(1-e^{-\lambda_{n,1}t})\frac{\sin(\sqrt{\lambda_{n,1}-k})}{\sqrt{\lambda_{n,1}-k}}\sin\left(\sqrt{\frac{\lambda_{n,1}-k_{en}}{D_{en}}}h_{en}\right)\right.$$

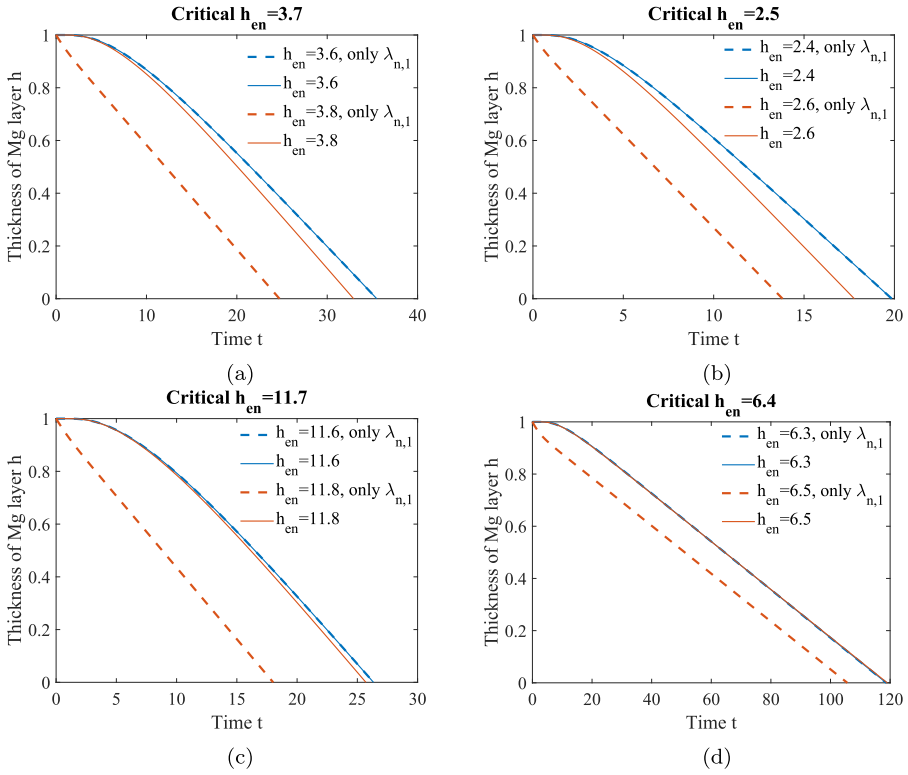

Fig. 2. The thickness of the Mg layer h versus time for (a) the baseline values $k = 0.18$, $D_{en} = 1$, and $k_{en} = 0$; (b) $k = 0.4$; (c) $D_{en} = 10$; (d) $k_{en} = 0.12$.

$$+\sum_n \frac{C_{n,2}}{\lambda_{n,2}}(1-e^{-\lambda_{n,2}t})\frac{\sinh(\sqrt{k-\lambda_{n,2}})}{\sqrt{k-\lambda_{n,2}}}\sin\left(\sqrt{\frac{\lambda_{n,2}-k_{en}}{D_{en}}}h_{en}\right)\Bigg], \quad k > k_{en} \tag{33}$$

$$h(t) = 1 - \frac{Mw_0}{q\rho M_w}k\Bigg[Pt\frac{\sinh(\sqrt{k})}{\sqrt{k}} + \sum_n \frac{C_{n,1}}{\lambda_{n,1}}(1-e^{-\lambda_{n,1}t})\frac{\sin(\sqrt{\lambda_{n,1}-k})}{\sqrt{\lambda_{n,1}-k}}\sin\left(\sqrt{\frac{\lambda_{n,1}-k_{en}}{D_{en}}}h_{en}\right) + \sum_n \frac{C_{n,2}}{\lambda_{n,2}}(1-e^{-\lambda_{n,2}t})\frac{\sin(\sqrt{\lambda_{n,2}-k})}{\sqrt{\lambda_{n,2}-k}}\sinh\left(\sqrt{\frac{k_{en}-\lambda_{n,2}}{D_{en}}}h_{en}\right)\Bigg], \quad k < k_{en} \tag{34}$$

2.6. Significance of the case $\lambda_{n,2}$

The effect of the eigenvalues $\lambda_{n,2}$, unaccounted for in prior studies (Li et al., 2013), is studied in this section for representative parameters $k = 0.18$ (Li et al., 2013), $D_{en} = 1$ (same diffusivity as the Mg layer), and $k_{en} = 0$ (no reaction in the encapsulation layer). The eigenvalues $\lambda_{n,2}$ come into play for $h_{en} > 3.7$, derived from Eq. (30). Fig. 2(a) shows the Mg layer thickness versus time. For $h_{en} = 3.8$, slightly above the critical value of 3.7, the curves with and without the eigenvalues $\lambda_{n,2}$ are far separated, indicating the importance to account for eigenvalues $\lambda_{n,2}$ for a relatively thick encapsulation. This observation also holds for other values of k, D_{en} and k_{en} deviating from their baseline values given above, such as $k = 0.4$ in Fig. 2(b) (while other parameters are fixed at the baseline values above), $D_{en} = 10$ in Fig. 2(c), and $k_{en} = 0.12$ in Fig. 2(d).

3. Scaling law for a thick encapsulation layer with no reaction

For an encapsulation layer with no reaction $k_{en} = 0$ and thickness

$$h_{en}/D_{en} \gg \coth\sqrt{k}/\sqrt{k} \tag{35}$$

the eigenvalues of the eigenequations Eq. (18) are obtained approximately but analytically (see the Appendix A). The time for the Mg layer thickness decrease Δh is also obtained analytically (see the Appendix A), and takes the form

$$t = \frac{h_{en}^2}{D_{en}} f\left(\frac{\Delta h}{h_{en}}\frac{q\rho M_w}{Mw_0}\right) \tag{36}$$

where f is a non-dimensional function given analytically in the Appendix A, and is shown in Fig. 3. It should be pointed out that this equation remains the same after the normalized variables (t and Δh) and parameters (h_{en} and D_{en}) are substituted by their dimensional counterparts according to Eq. (2). The above equation gives the scaling law between the dissolution time t and dissolved thickness of the Mg layer Δh. The numerical results show that, for $h_{en}/D_{en} > 100$, the dissolution time obtained from the double-layer model in Section 2 is less than 10% different from the scaling law in Eq. (36). The term "thick" used in our previous discussions refers not merely to a large value of dimensionless h_{en} but more accurately to a large ratio of h_{en}/D_{en} (Eq. (35)), where h_{en} and D_{en} are all dimensionless. The scaling law remains applicable even to encapsulation layers with relatively modest thickness but low diffusivity.

4. Conclusion remarks

We have extended Li et al.'s analytical model of reactive diffusion for transient electronics (Li et al., 2013) to account for the effect of

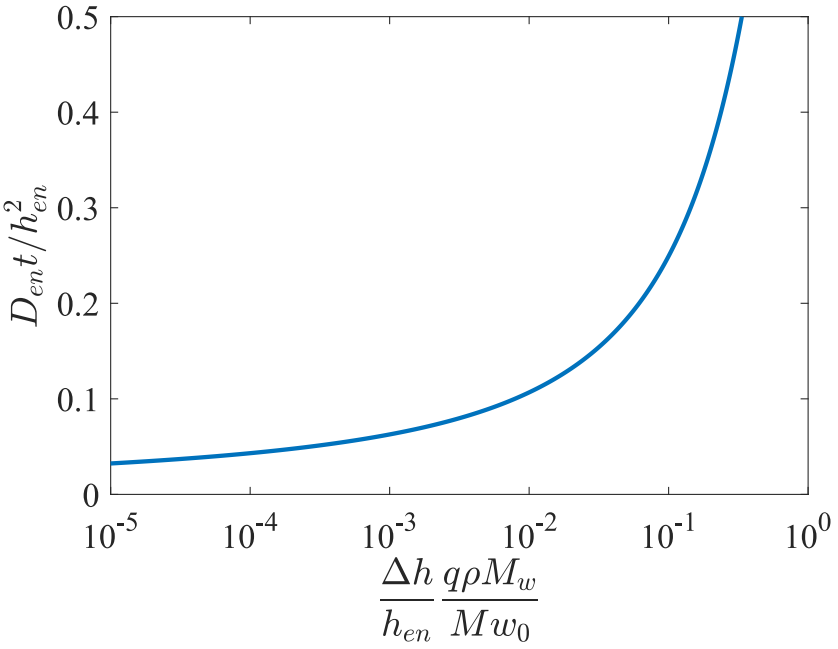

Fig. 3. The scaling law that relates $\frac{D_{en}t}{h_{en}^2}$ and $\frac{\Delta h}{h_{en}}\frac{q\rho M_w}{Mw_0}$.

relatively thick encapsulation. It gives a critical thickness of the encapsulation layer, above which our results can be substantially different from those of Li et al. (2013). We have also established a scaling law for the dissolution time of a thick encapsulation layer with no reaction. It provides a rather robust way to estimate the dissolution time.

CRediT authorship contribution statement

Haohui Zhang: Conceptualization, Methodology, Validation, Formal analysis, Investigation, Writing – original draft, Writing – review & editing, Visualization. **Kaiqing Zhang:** Formal analysis, Investigation, Writing – review & editing. **John A. Rogers:** Conceptualization, Writing – review & editing, Supervision. **Yonggang Huang:** Conceptualization, Methodology, Validation, Formal analysis, Investigation, Resources, Writing – original draft, Writing – review & editing, Supervision, Project administration.

Declaration of competing interest

The authors declare that they have no known competing financial interests or personal relationships that could have appeared to influence the work reported in this paper.

Data availability

Data will be made available on request.

Appendix A. Analytical solution for a thick encapsulation layer with no reaction

For $k_{en} = 0$ and a thick encapsulation layer satisfying Eq. (35), the eigenvalues of the eigenequation Eq. (18) can be solved approximately as $\lambda_{n,2} = \frac{D_{en}}{h_{en}^2}n^2\pi^2$, $n = 1, 2, \ldots, n_m$. Here $n_m = \left\lfloor \sqrt{\frac{k}{D_{en}}}\frac{h_{en}}{\pi} \right\rfloor$ denotes the number of eigenvalues satisfying $\lambda_{n,2} < k$, where $\lfloor\ \rfloor$ is the floor function. For a thick encapsulation layer, n_m becomes very large, the coefficient $C_{n,1}$ becomes essentially zero, and the coefficient $C_{n,2}$ is given by $\frac{2}{n\pi\cosh\sqrt{k}}$. The dissolved thickness of the Mg layer is then given by

$$\frac{\Delta h}{h_{en}} = \frac{Mw_0}{q\rho M_w}\left[\frac{D_{en}t}{h_{en}^2} + \sum_{n=1}^{\infty}\frac{2(-1)^n}{n^2\pi^2}\left(1 - e^{-\frac{n^2\pi^2 D_{en}t}{h_{en}^2}}\right)\right] \tag{A.1}$$

The equation then leads to the scaling law in Eq. (36).

Appendix B. Comparison between the scaling law and the double-layer model

To validate the scaling law, we compare it with the double-layer model outlined in Section 2, utilizing parameters $k = 0.18$, $D_{en} = 1$, and $h_{en} = 100$ (Fig. B.4). Two curves exhibit minimal discrepancies, showing the effectiveness of our scaling law as a robust approximation for thick encapsulation layers.

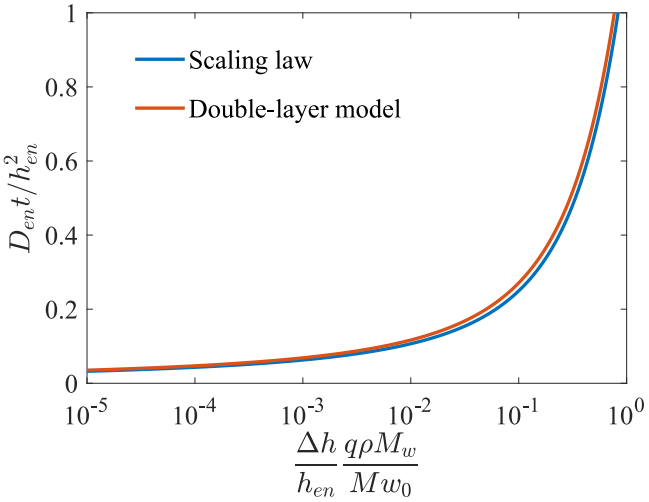

Fig. B.4. Comparison between the scaling law and the double-layer model under the parameters: $k = 0.18$, $D_{en} = 1$, and $h_{en} = 100$.

References

Amaral, L., Oliveira, I., Salomão, R., Frollini, E., Pandolfelli, V., 2010. Temperature and common-ion effect on magnesium oxide (MgO) hydration. Ceram. Int. 36 (3), 1047–1054.

Badawy, W., Al-Kharafi, F., 1998. Corrosion and passivation behaviors of molybdenum in aqueous solutions of different pH. Electrochim. Acta 44 (4), 693–702.

Bowen, P.K., Drelich, J., Goldman, J., 2013. Zinc exhibits ideal physiological corrosion behavior for bioabsorbable stents. Adv. Mater. 25 (18), 2577–2582.

Burns, K.N., Sun, K., Fobil, J.N., Neitzel, R.L., 2016. Heart rate, stress, and occupational noise exposure among electronic waste recycling workers. Int. J. Environ. Res. Public Health 13 (1), 140.

Choi, Y.S., Koo, J., Lee, Y.J., Lee, G., Avila, R., Ying, H., Reeder, J., Hambitzer, L., Im, K., Kim, J., et al., 2020. Biodegradable polyanhydrides as encapsulation layers for transient electronics. Adv. Funct. Mater. 30 (31), 2000941.

Fu, K.K., Wang, Z., Dai, J., Carter, M., Hu, L., 2016. Transient electronics: materials and devices. Chem. Mater. 28 (11), 3527–3539.

Heacock, M., Kelly, C.B., Asante, K.A., Birnbaum, L.S., Bergman, Å.L., Bruné, M.-N., Buka, I., Carpenter, D.O., Chen, A., Huo, X., et al., 2016. E-waste and harm to vulnerable populations: a growing global problem. Environ. Health Perspect. 124 (5), 550–555.

Hermawan, H., Purnama, A., Dube, D., Couet, J., Mantovani, D., 2010. Fe–Mn alloys for metallic biodegradable stents: degradation and cell viability studies. Acta Biomater. 6 (5), 1852–1860.

Huang, X., Liu, Y., Hwang, S.-W., Kang, S.-K., Patnaik, D., Cortes, J.F., Rogers, J.A., 2014. Biodegradable materials for multilayer transient printed circuit boards. Adv. Mater. 26 (43), 7371–7377.

Hwang, S.-W., Tao, H., Kim, D.-H., Cheng, H., Song, J.-K., Rill, E., Brenckle, M.A., Panilaitis, B., Won, S.M., Kim, Y.-S., et al., 2012. A physically transient form of silicon electronics. Science 337 (6102), 1640–1644.

Iler, R., 1973. Effect of adsorbed alumina on the solubility of amorphous silica in water. J. Colloid Interface Sci. 43 (2), 399–408.

Irimia-Vladu, M., Troshin, P.A., Reisinger, M., Shmygleva, L., Kanbur, Y., Schwabegger, G., Bodea, M., Schwödiauer, R., Mumyatov, A., Fergus, J.W., et al., 2010. Biocompatible and biodegradable materials for organic field-effect transistors. Adv. Funct. Mater. 20 (23), 4069–4076.

Jia, X., Wang, C., Zhao, C., Ge, Y., Wallace, G.G., 2016. Toward biodegradable Mg–air bioelectric batteries composed of silk fibroin–polypyrrole film. Adv. Funct. Mater. 26 (9), 1454–1462.

Jung, Y.H., Chang, T.-H., Zhang, H., Yao, C., Zheng, Q., Yang, V.W., Mi, H., Kim, M., Cho, S.J., Park, D.-W., et al., 2015. High-performance green flexible electronics based on biodegradable cellulose nanofibril paper. Nat. Commun. 6 (1), 7170.

Kang, S.-K., Hwang, S.-W., Cheng, H., Yu, S., Kim, B.H., Kim, J.-H., Huang, Y., Rogers, J.A., 2014. Dissolution behaviors and applications of silicon oxides and nitrides in transient electronics. Adv. Funct. Mater. 24 (28), 4427–4434.

Kang, S.-K., Murphy, R.K., Hwang, S.-W., Lee, S.M., Harburg, D.V., Krueger, N.A., Shin, J., Gamble, P., Cheng, H., Yu, S., et al., 2016. Bioresorbable silicon electronic sensors for the brain. Nature 530 (7588), 71–76.

Krauskopf, K.B., 1956. Dissolution and precipitation of silica at low temperatures. Geochim. Cosmochim. Acta 10 (1–2), 1–26.

Lee, C.H., Kim, H., Harburg, D.V., Park, G., Ma, Y., Pan, T., Kim, J.S., Lee, N.Y., Kim, B.H., Jang, K.-I., et al., 2015. Biological lipid membranes for on-demand, wireless drug delivery from thin, bioresorbable electronic implants. NPG Asia Mater. 7 (11), e227.

Lee, Y.K., Yu, K.J., Kim, Y., Yoon, Y., Xie, Z., Song, E., Luan, H., Feng, X., Huang, Y., Rogers, J.A., 2017. Kinetics and chemistry of hydrolysis of ultrathin, thermally grown layers of silicon oxide as biofluid barriers in flexible electronic systems. ACS Appl. Mater. Interfaces 9 (49), 42633–42638.

Li, R., Cheng, H., Su, Y., Hwang, S.-W., Yin, L., Tao, H., Brenckle, M.A., Kim, D.-H., Omenetto, F.G., Rogers, J.A., et al., 2013. An analytical model of reactive diffusion for transient electronics. Adv. Funct. Mater. 23 (24), 3106–3114.

Mueller, P.P., Arnold, S., Badar, M., Bormann, D., Bach, F.-W., Drynda, A., Meyer-Lindenberg, A., Hauser, H., Peuster, M., 2012. Histological and molecular evaluation of iron as degradable medical implant material in a murine animal model. J. Biomed. Mater. Res. Part A 100 (11), 2881–2889.

Nie, F., Zheng, Y., Wei, S., Hu, C., Yang, G., 2010. In vitro corrosion, cytotoxicity and hemocompatibility of bulk nanocrystalline pure iron. Biomed. Mater. 5 (6), 065015.

Patrick, E., Orazem, M.E., Sanchez, J.C., Nishida, T., 2011. Corrosion of tungsten microelectrodes used in neural recording applications. J. Neurosci. Methods 198 (2), 158–171.

Place, E.S., George, J.H., Williams, C.K., Stevens, M.M., 2009. Synthetic polymer scaffolds for tissue engineering. Chem. Soc. Rev. 38 (4), 1139–1151.

Rimstidt, J.D., Barnes, H., 1980. The kinetics of silica-water reactions. Geochim. Cosmochim. Acta 44 (11), 1683–1699.

Tao, H., Hwang, S.-W., Marelli, B., An, B., Moreau, J.E., Yang, M., Brenckle, M.A., Kim, S., Kaplan, D.L., Rogers, J.A., et al., 2014. Silk-based resorbable electronic devices for remotely controlled therapy and in vivo infection abatement. Proc. Natl. Acad. Sci. 111 (49), 17385–17389.

Wetteland, C.L., de Jesus Sanchez, J., Silken, C.A., Nguyen, N.-Y.T., Mahmood, O., Liu, H., 2018. Dissociation of magnesium oxide and magnesium hydroxide nanoparticles in physiologically relevant fluids. J. Nanopart. Res. 20, 1–17.

Witte, F., 2010. The history of biodegradable magnesium implants: a review. Acta Biomater. 6 (5), 1680–1692.

Won, S.M., Koo, J., Crawford, K.E., Mickle, A.D., Xue, Y., Min, S., McIlvried, L.A., Yan, Y., Kim, S.B., Lee, S.M., et al., 2018. Natural wax for transient electronics. Adv. Funct. Mater. 28 (32), 1801819.

Yin, L., Cheng, H., Mao, S., Haasch, R., Liu, Y., Xie, X., Hwang, S.-W., Jain, H., Kang, S.-K., Su, Y., et al., 2014. Dissolvable metals for transient electronics. Adv. Funct. Mater. 24 (5), 645–658.

Yu, K.J., Kuzum, D., Hwang, S.-W., Kim, B.H., Juul, H., Kim, N.H., Won, S.M., Chiang, K., Trumpis, M., Richardson, A.G., et al., 2016. Bioresorbable silicon electronics for transient spatiotemporal mapping of electrical activity from the cerebral cortex. Nat. Mater. 15 (7), 782–791.

Zeng, R., Dietzel, W., Witte, F., Hort, N., Blawert, C., 2008. Progress and challenge for magnesium alloys as biomaterials. Adv. Eng. Mater. 10 (8), B3–B14.